*Russian Chemical Reviews* **75** (1) 23 – 30 (2006) © 2006 Russian Academy of Sciences and Turpion Ltd

DOI 10.1070/RC2006v075n01ABEH003600

# Atomic resolution probe microscopy of the graphite surface

O V Sinitsyna, I V Yaminsky

## Contents


| | | |
|---|---|---|
| I. | Introduction | 23 |
| II. | Crystal structure of graphite | 23 |
| III. | Visualisation of the atomic structure of graphite surface | 24 |
| IV. | Defects on the graphite surface | 27 |
| V. | Conclusion | 29 |


**Abstract. The results of theoretical and experimental studies of the graphite surface by scanning tunnelling and atomic force microscopy are considered. The attention is focused on the mechanisms of formation of atomic resolution images. The reasons for the lack of coincidence between the graphite surface images obtained by these methods and its real topography are discussed. The bibliography includes 99 references.**

## I. Introduction

Graphite has an extremely wide range of applications. It is employed as a material for inert electrodes, neutron moderators, X-ray monochromators, strong and thermally stable coatings for spacecrafts. Technical progress has stimulated the development of new technologies of graphite production, as well as massive studies of its chemical and physical properties. In the early 1970's, it was believed that graphite is studied comprehensively. The known data were generalised in a number of reviews (see, for example, Refs 1 – 3).

In the 1980's, new instruments for surface studies were invented, such as scanning tunnelling microscope (STM)[4] and atomic force microscope (AFM).[5] Studies of graphite by these novel probe methods gave amazing results: its STM and AFM images were inconsistent with the real topography. Only one of each two carbon atoms was visible on the image. During the next decades a lot of studies were conducted in order to explain this fact. Despite the great amount of experimental data collected, there is still no consensus on the mechanism of the formation of STM images with atomic resolution.

Graphite crystals are convenient objects for the rapidly developing probe microscopy, as they have layered structure and form air-stable, atomic-smooth extended surfaces upon cleavage. Therefore they can be used as substrates in the studies of clusters, molecules and thin films. Graphite is one of a few materials for which atomic resolution was reached under normal conditions in air.

At present, probe methods play a leading role in studies of surfaces. The portion of surface atoms in nanostructures is comparable to their volume content, therefore probe microscopy is an indispensable method in nanotechnology. Probe microscopes allow one to obtain images in liquid media, which is especially valuable in the studies of biological objects. However, STM and AFM images can differ from the topography of surfaces of the objects under study. Difficulties in the interpretation of graphite surface images suggest that one may expect serious errors in the studies of more complex systems.

In this review, the graphite atomic structure images observed with the use of STM and AFM in a contact or dynamic mode are analysed in detail. (In the contact mode, the probe is constantly in touch with the surface, while in the dynamic mode it oscillates in resonance and touches the surface periodically, thus minimising the friction force.) The mechanisms of formation of such images are discussed. A separate section is devoted to the visualisation of defects on the graphite surface and studies of their properties by probe methods.

## II. Crystal structure of graphite

Among the carbon allotropic modifications, graphite is the most stable under normal conditions. Graphite consists of flat carbon layers that are shifted relative to each other to form hexagonal close packing of carbon atoms (Fig. 1 *a*). The space group is $P6_3/mmc$ and the unit cell parameters are: $a = 2.4612$, $c = 6.7078$ Å.[6] The unit cell contains four atoms. Two adjacent carbon atoms in the layer are non-equivalent (see Fig. 1 *b*). Three of the six atoms have neighbours in the lower layer (site A), while

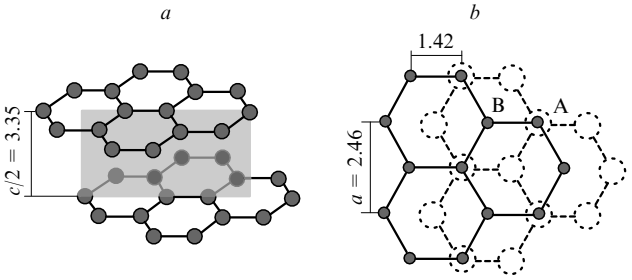



**Figure 1.** Graphite crystal structure.
The unit cell parameters are given in Ångströms; for (*a*) and (*b*) see the text.

**O V Sinitsyna** Department of Materials Science, M V Lomonosov Moscow State University, Leninskie Gory, 119992 Moscow, Russian Federation. Fax (7-495) 939 09 98, e-mail: sinitsyna@gmail.com
**I V Yaminsky** Department of Physics, M V Lomonosov Moscow State University, Leninskie Gory, 119992 Moscow, Russian Federation. Fax (7-495) 939 10 09, tel. (7-495) 939 29 82, e-mail: yaminsky@nanoscopy.org

Received 25 August 2005
*Uspekhi Khimii* **75** (1) 27 – 35 (2006); translated by I S Neretin

other three are located above the holes, *i.e.* in the centres of hexagons (site B). Weak van der Waals forces act between layers, causing substantial anisotropy of the graphite properties. Thermal and electrical conductivities in the direction parallel to the layers are much higher than in the perpendicular direction (Table 1). Due to the weakness of the interlayer bonds, graphite is easy to cleave.

**Table 1**. Electric resistance and thermal conductivity of highly oriented pyrolytic graphite (HOPG) and single-crystal graphite.[2]

| Parameter | HOPG | Single crystal |
|---|---|---|
| Resistance /Ω m | | |
| along the layers | $3.5\times10^{-7}-4.5\times10^{-7}$ | $4\times10^{-7}$ |
| perpendicular to the layers | $1.5\times10^{-3}-2.5\times10^{-3}$ | $1\times10^{-4}-1.0\times10^{-2}$ |
| Thermal conductivity /W m$^{-1}$ K$^{-1}$ | | |
| along the layers | 1600 – 2000 | 200 – 500 |
| perpendicular to the layers | 7 – 9 | 40 – 80 |

Graphite crystals of high quality are rarely found in nature. At present, most of the studies are carried out on highly oriented pyrolytic graphite, which is obtained by pyrolysis of gaseous hydrocarbons at temperatures above 2000 °C.[2,7,8] Graphite obtained by this method is polycrystalline; however the directions of *c* axes for all crystallites virtually coincide (mosaic spread of high quality pyrolytic graphite is 0.4°, the dimensions of crystallites reach several tens of micrometers).

## III. Visualisation of the atomic structure of graphite surface

### 1. Scanning tunnelling microscopy

Atomic resolution STM images of the graphite surface were obtained under different conditions: in high vacuum [9–11] (Fig. 2, the real image size is not given in the original paper), in air [12–15] and in water.[13,16] The resolution is atomic that indeed is supported by the possibility to visualise defects in the atomic structure of the graphite surface by STM (Fig. 3).

Two main peculiarities of the graphite surface STM images are as follows:[18–21] considerable corrugation of the surface (from 0.8 [22,23] to 24 Å [24]) and asymmetry of the maxima corresponding to the carbon atoms in sites A and B.

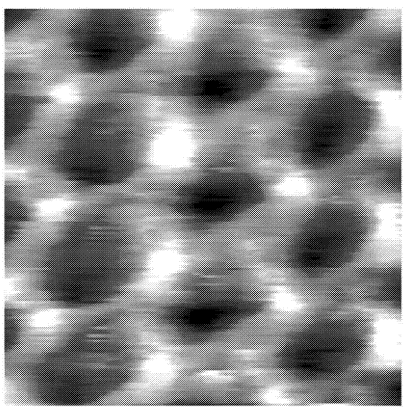


**Figure 2.** Topographic graphite image obtained by STM in ultrahigh vacuum at 4.2 K.[11]

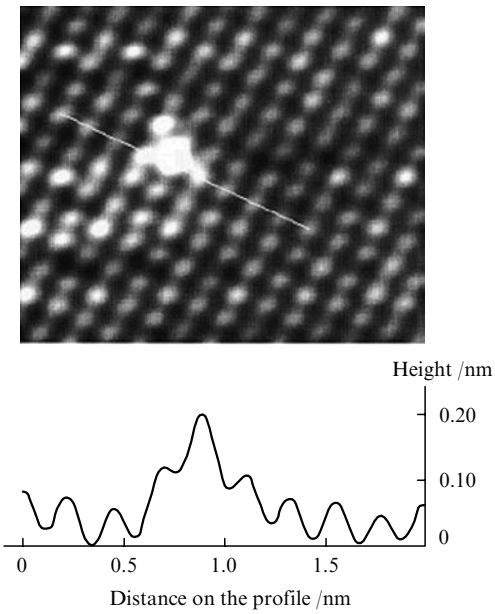



**Figure 3.** A defect on the graphite surface induced by its bombardment with $Ar^+$ at 60 eV.[17]
The image was obtained in the constant-current mode, $U = -36$ mV, $I = 0.5$ nA, scanning frequency, 10 Hz.

According to the helium scattering experiments, no surface reconstruction occurs and its corrugation is 0.2 Å. The overestimated corrugation obtained by the scanning tunnelling microscopy is due to the features of graphite electronic structure,[13,25] as well as to the effect of the microscope tip on the surface during scanning.[24,26,27] An increase in the tip voltage leads to decrease in the corrugation.[9,28]

A very interesting feature of the graphite surface STM images is the non-equivalence of the maxima corresponding to the adjacent carbon atoms.[14,29] In some experiments, the asymmetry is so great that only three of the six atoms can be seen (a triangular array in Fig. 4 *a*), in other cases all six atoms are observed with equal intensities (carbon hexagons in Fig. 4 *b*).

There are several concepts of this asymmetry.

1. According to the theory of Tomanek *et al.*,[15,30] asymmetry of the tunnelling current at low voltages is related to the difference in the local density of states, which, in the case of graphite, is determined by the interlayer interaction and the structural non-equivalence of the atomic positions. The calculations have shown [31] that the maxima in the STM images correspond to the atoms in the sites B. According to this theory, the tunnelling current asymmetry should decrease with the increase in voltage, but should not be sensitive to its polarity. This was proven experimentally.[15,30] For alkali metal intercalates, where carbon layers are arranged exactly one over the other and therefore all carbon atoms are equivalent, this theory predicts the absence of asymmetry.

In the STM image of alkali metal intercalates (Li, K, Rb, Cs), different lattices were revealed. Their periods are determined by the arrangement of the intercalated atoms (Fig. 5).[23,31] This feature complicates the analysis of the carbon atom asymmetry.

The graphite lattice was successfully visualised for acceptor intercalation compounds.[32] For example, different lattices were observed for $MoCl_5$-intercalated graphite within one image, namely, a trigonal lattice of maxima in non-intercalated areas and a honeycomb network of hexagons in the areas containing molybden pentachloride molecules in the first interlayer space (Fig. 6).[33]

Within the framework of Tomanek's theory, the absence of the asymmetry can be explained by the shift of the top layer with

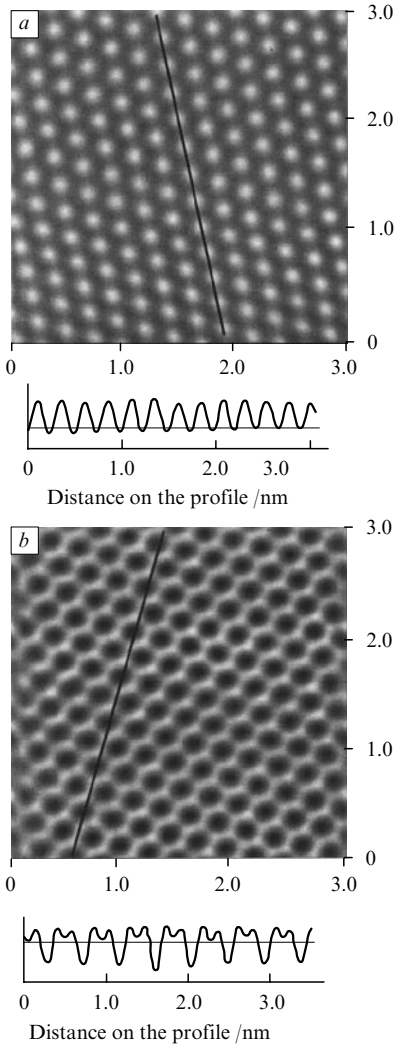



**Figure 4.** HOPG images with atomic resolution obtained by STM ($U = 20$ mV, $I = 1$ nA).[14]
Scanning frequency /Hz: 61 (*a*) and 122 (*b*).

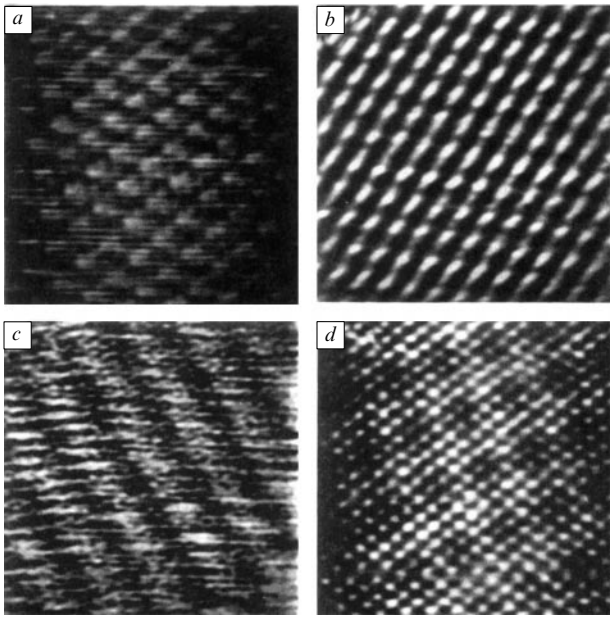



**Figure 5.** Images of the intercalate $C_8K$ surface obtained by STM.[30] (*a*) constant-height mode ($5 \times 5$ nm$^2$, $I = 3.5$ nA, $U = -20$ mV), a hexagonal $2 \times 2$ superlattice is visible; (*b*) constant-current mode ($5 \times 5$ nm$^2$, $I = 5$ nA, $U = -50$ mV), a hexagonal $\sqrt{3} \times \sqrt{3}$ superlattice is visible; (*c*) constant-current mode ($20 \times 20$ nm$^2$, $I = 10$ nA, $U = -19$ mV), a superlattice with the period of 3.3 nm is visible; (*d*) constant-height mode ($5 \times 5$ nm$^2$, $I = 3.5$ nA, $U = -20$ mV), an orthorhombic superlattice with the period of 0.95 nm is visible.

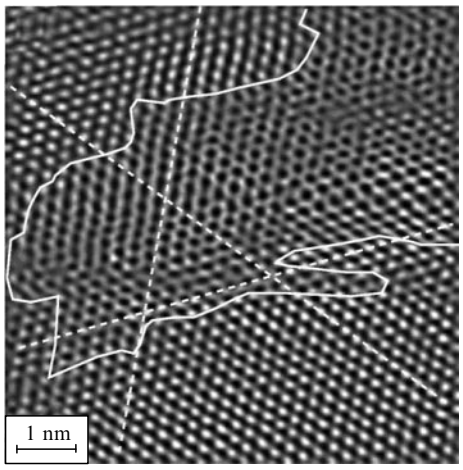



**Figure 6.** Surface image of the HOPG intercalated with $MoCl_5$ obtained by STM in the constant-height mode.[33]

respect to the lower layers during scanning. Indeed, the change in the character of image in the majority of cases was caused by passage to more 'drastic' [14] scanning conditions, *viz*. an increase in the tunnelling current or a decrease in the voltage between the tip and the sample. Moreover, in one experiment [14] a change in the image type was observed with the change in the scanning speed in the constant height mode (see Fig. 4).

Evolution of the graphite surface image during scanning was described.[34] First scans have shown the asymmetry of maxima (A : B = 4 : 7). During the next scans, the image gradually changed until complete disappearance of asymmetry. However, on further measurements, the maxima became asymmetric again with a minimum A : B ratio. Probably, changes in the image during scanning are caused by sliding of the top layer relative the lower layers. This sliding should occur easier in the area near to a defect, such as dislocation or vacancy. Since scanning covers a very small area, the probability of its position in the vicinity of the defect is rather low. This explains the rare appearance of the honeycomb structure.[14]

2. The main point of an alternative theory is that the A and B sites differ in their rigidities.[35] In other words, the perpendicular shift of a carbon atom in the site B requires more energy than similar shift of an atom in the site A; thus the site B is more 'rigid'. Mechanical pressure of the STM tip on the graphite surface can result in the deformation of the layer and local changes in the tunnelling threshold. Therefore, in the case of repulsion forces the maxima on the image should correspond to the positions of the greatest rigidity. Because of the relatively large radii of the tip material atoms (W, Pt, Ir), which are comparable to the side of the carbon hexagon, it is necessary to take into account the interaction of probe not only with the carbon atom located directly below it, but also with the neighbouring atoms. In this case, the position of the maximum rigidity can be located in the hexagon centre and the maxima of the detected value in the image correspond to the holes.[22]

Whereas the difference in the tunnelling current is determined in general by the 'rigidity' of positions, the appearance of all six atoms in the STM image with equal intensities can be explained by the selection of 'soft' scanning conditions where the surface

deformation is minimal. For example, a tiny particle of graphite can become attached to the tip, or the tip-to-sample distance is fairly large.[22]

3. The asymmetry of carbon atoms is caused by the formation of charge density waves.[36] However, according to this theory, the asymmetry value should depend on the polarity of the tunnelling voltage, which contradicts the experimental data.

4. Tunnelling can occur through the local surface states. In this case, the change in the image depending on the variation of the tunnelling current by several tenth of nanoampers can be explained by the presence of an adsorbate on the graphite surface.[37]

Based on the theories 1 and 2, the difference in the intensities of maxima corresponding to the carbon atoms in A and B sites is determined by the influence of lower layers. According to theory 2, this influence is manifested in the deformation of the surface by the probe. Taking this into account, it can be predicted that in the case of scanning of a graphene (single graphite layer) the asymmetry should be absent. However, such a conclusion contradicts the available data [38] on the observation of only three of the six atoms in an STM image of a single graphene layer on the Pt(111) surface with atomic resolution. The isolated single graphene layer is extremely difficult to obtain,[39] therefore the graphene properties remain almost unknown so far. It is still possible that the STM image of the graphite surface is determined solely by the properties of one layer.

## 2. Atomic force microscopy

Graphite atomic structure images obtained in contact and dynamic modes of AFM differ substantially. In the contact mode, it is possible to detect only the graphite unit cell as a whole (Fig. 7), but at the same time, measurements can be carried out at ambient conditions.[41–43] In the contact mode, the friction forces dominate, therefore this variant of AFM is an indispensable tool for nanotribology.

A different situation takes place in the case of dynamic AFM. This allows visualisation of separate atoms on the graphite surface. However, the atomic resolutions can be reached only under ultrahigh vacuum at helium temperatures and using perfect vibroisolation.[44,45] This is due to the fact that the graphite surface is relatively inert in comparison with the ionic surfaces or to the surfaces with 'dangling' bonds. The forces applied to the tip near the graphite surface are of about $\sim 100$ pN.

Let us discuss the main mechanisms of formation of AFM images of the graphite surface obtained in the contact mode, *viz*. in the stick-slip motion of the tip [43,46,47] and in scanning with a modified tip (when a graphite flake is attached to the tip).[48–50] In a number of theoretical works, the influence of probe geometry on the scanning process is considered.[46,51–53]

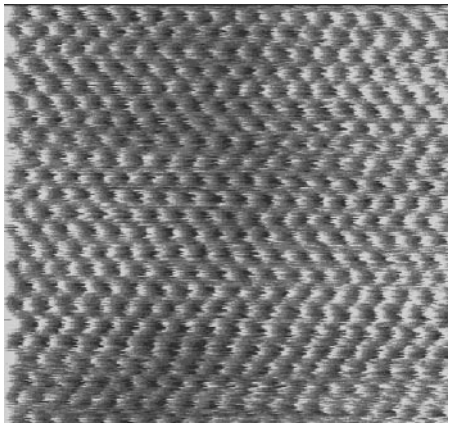


**Figure 7.** Image of the HOPG surface obtained by AFM in the contact mode with the friction force detection.[40]
The normal force component is 40 nN, scanning frequency is 30 Hz.

Now let us analyse the reasons why the tip moves with sticking while it is in the contact with the graphite surface. According to published data,[46] we will consider the dependence of the potential energy of a single-atom tip – a single graphite layer system versus the tip position relative to the sample. The virtual scanning takes place in the constant height mode at $-6$ Å, therefore the normal component of the force acting between the surface and the tip is repulsive. In the scanning with the sufficiently rigid cantilever (the rigidity constant for this model was 1.3 N m$^{-1}$), the potential energy of the system has one minimum. In the case of a soft cantilever, an additional local minimum appears. Transition from the local to the global minimum is accompanied by a drastic change in the friction force. The tip sticks in hexagon centres and its move from one hexagon centre to another occurs in jumps.[43,46] Continuous motion is possible in the case of more rigid cantilever or more 'flat' potential of the tip-to-surface interaction, but these conditions are not met in the experiment.[40,46]

Calculations have shown [54] that a single-atom tip pressed against the graphite surface with a force of *ca.* $\sim 1$ nN bends it by 1 Å. The deformation extends only to the first three layers. Surface curvature disappears at a characteristic length of $\sim 10$ Å. The influence of a many-atomic tip should span the larger area of the graphite surface.[55] In some situations, the tip as a whole is attracted to the surface, but its topmost atom is in the area of repulsive force, thus causing plastic deformation of the graphite surface.[52]

Measurements carried out in liquid media allow a decrease in the contribution of long-distance macroscopic forces acting between the peripheric atoms of the tip and the graphite surface. Presumably,[56] under such conditions one can obtain more stable images, although the contrast for the images obtained in the liquid is lower than for those obtained in vacuum (the difference in maximum heights is 0.39 and 0.6 Å, respectively).

Periodic changes in the friction forces during scanning can also be explained by modification of the tip as a result of sticking of a graphite flake to the tip. The friction force of $\sim 1$ nN, which appears at the shift of a modified probe to the new equilibrium position, is due to the interaction of the sample surface with the cluster (flake) consisting of *ca.* $\sim 100$ carbon atoms. The radius of the contact area does not exceed 1 nm.[50] When moved along the direction $\langle 12\bar{3}0 \rangle$, the graphite flake moves rectilinearly together with the probe, while in the scanning in other directions, the tip with the particle moves in a zigzag manner [50] or the flake is reoriented according to the direction of the tip rectilinear motion.[49] In these cases, from the AFM images it is possible to determine whether the tip has been modified.[50] For example, an AFM image of the graphite surface in the widely cited work by Mate *et al*.[41] should be classified as the one obtained with modified cantilever.

In the dynamic mode, features of the AFM image are determined by the character of forces acting between the probe and the sample.[51] An AFM image of the graphite surface obtained in the dynamic mode while detecting the repulsion forces is presented in Fig. 8. Two forces applied to the probe from the two adjacent carbon atoms are measured to be 248 and 250 pN. Obviously, the structural non-equivalence of the carbon atoms in graphite is manifested in the atomic force microscopy as well.

A substantial asymmetry between the atoms can be seen in the graphite surface image obtained by detection of the attractive forces.[58] According to the theory by Chen,[59] the attractive force acting on the tip should unequivocally determine the tunnelling current. In this case, the attraction force is a minimum for the tip position above the hexagon centre, and hence such a position corresponds to the maximum in the AFM image.[60] Atoms in the site A give weak local maxima, while atoms in the site B correspond to minima. Thus, the contrast in AFM images of graphite surface is inverted with respect to the STM images.

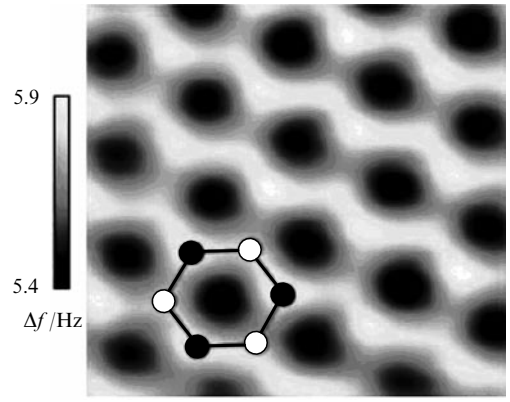



**Figure 8.** Graphite surface image obtained by AFM in the dynamic mode.[57]
Probe oscillation amplitude is 300 pm, scanning speed is 0.2 nm $s^{-1}$; white and black circles denote carbon atoms in A and B sites, respectively.

For the verification of Chen's theory, scanning was performed in the constant-height mode. The tunnelling current, the force acting on the tip and the dissipated energy were detected simultaneously (Fig. 9).[10] It was expected that the maxima of the tunnelling current should correspond to the carbon atoms in the B sites, while the dissipated energy should be maximum upon the holes. It was established that in the case of repulsive forces (see Fig. 9 *c*,† *f*) the asymmetry is a minimum, the maximum of the force corresponds to the atoms in sites A and the minimum corresponds to the holes. In the case of scanning in the attractive forces zone (see Fig. 9 *a*,*d*), the force depended on the voltage applied to the tip. At negative bias voltage of −60 mV, images based on the measurement of tunnelling current and the attractive force were inverted, in qualitative accordance with the Chen theory. However, no inversion occurred in the case of scanning at positive potential of +160 mV (see Fig. 9 *a*).

## IV. Defects on the graphite surface

Probe methods allow studying of not only the composition of defects and their electronic structures, but also their reactivities. By means of scanning tunnelling microscopy, it is possible to determine the electron energy spectra or to establish the nature of an admixture atom.[59]

First let us consider point defects, *i.e.*, vacancies and admixture atoms. The concentration of point defects on the HOPG surface of different quality under normal conditions is 0.1–20 $\mu m^{-2}$ (Refs 61 and 62). Defects appear in the STM images as bright spots (see Fig. 3).[19,20] When the tip approaches the surface, the defects become invisible, as the volume states of graphite make the main contribution to the tunnelling process under these conditions. Judging by the dependence of the defect height from the tip-to-sample distance, one can determine the type of the incorporated atom.[19,20]

In the majority of works, the point defects for their subsequent study are created artificially, usually by means of graphite surface bombardment with different ions.[17,63–66] Such a process can lead to the vacancy formation on the surface layer, as well as to the implantation of ions. Local density of states at the vicinity of the vacancy increases, making them visible in STM images, but not in AFM images.[17] Structure relaxation around the point defect can lead to the formation of new bonds, including those between atoms from adjacent layers.[67] But changes in the surface topography are too subtle to be detected by AFM working in the contact mode. The increase in the charge density occurring around the vacancy[17] explains the increased reactivity of the defect area.[68–70]

Ion implantation leads to the formation of dome-shaped structures[65] and craters on the surface.[63] After heating of the ion-implanted samples at 500 °C, the height of the defect area

† The insert in Fig. 9 *c* on the left shows a higher harmonic image.

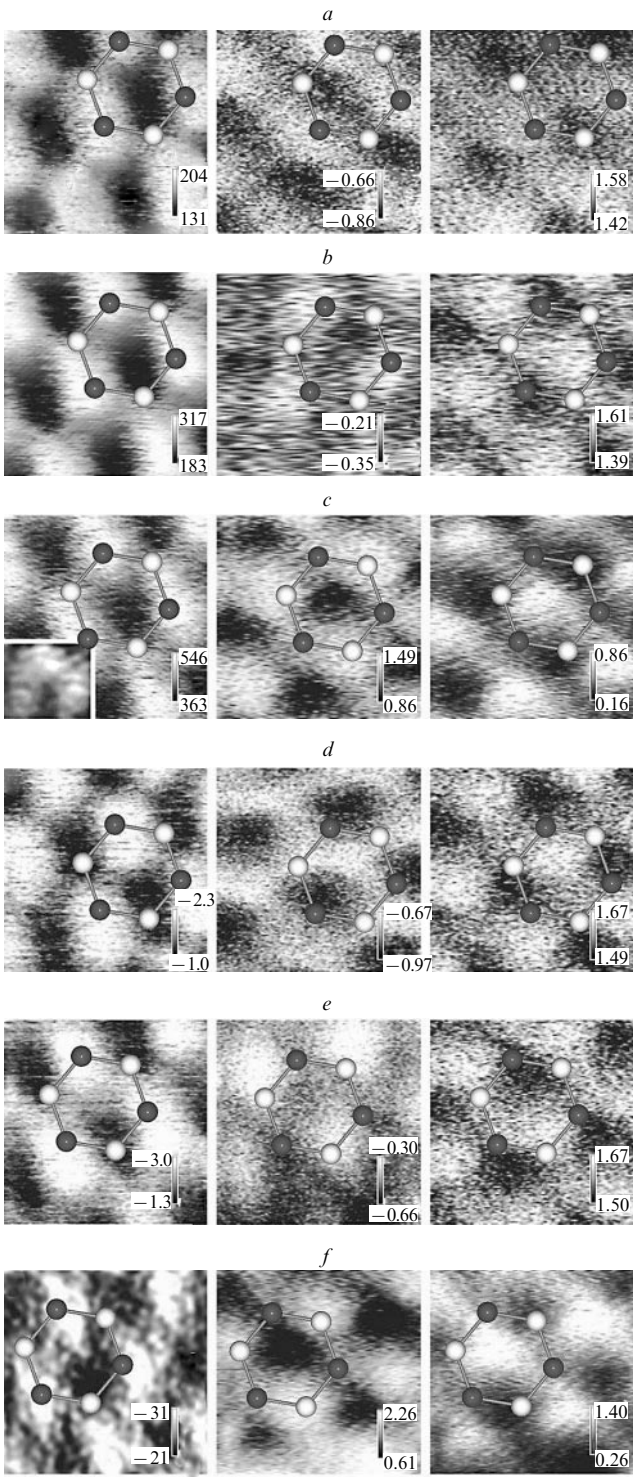



**Figure 9.** HOPG surface images obtained in the constant-height mode.[10] The tunnelling current (pA) was measured for the images to the left; a normalised shift of the resonance frequency (fN $m^{1/2}$) in the middle, and the dissipated energy (eV) to the right.
*U* /mV: 160 (*a*–*c*), −60 (*d*–*f*); *z* /pm: −100 (*a*, *d*), −350 (*b*, *e*), −750 (*c*, *f*).

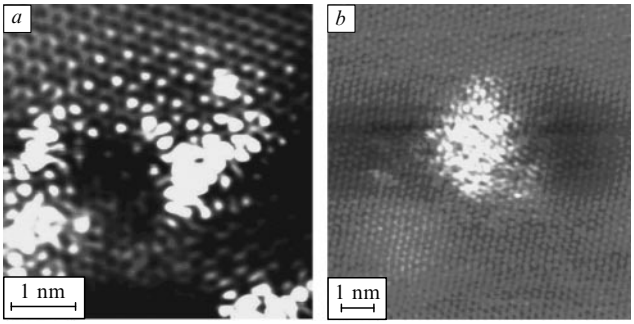



**Figure 10.** Atomic resolution images of the HOPG surface with implanted tungsten ions obtained by STM.[63]
Switch of the polarity of the tunnelling voltage did not reveal any new features in the image.

increases, which can be explained by the migration of the implanted ions closer to the surface.[63]

In STM images of graphite around point defects, as well as at step edges, the formation of $\sqrt{3} \times \sqrt{3}\boldsymbol{R}\,30^\circ$ structure was observed (Fig. 10). This is not due to surface reconstruction,[71,72] but can be explained by the Friedel oscillations.[73] Analysis of their symmetry allows one to establish the nature of point defects and the adsorbate state.[19,20] For example, with account of the enhancement of the Friedel oscillation amplitude, the formation of covalent C–F bond on the graphite surface was concluded.[74]

Possible line defects in cleaved HOPG include steps,[75] domain borders[76] and dislocations. The steps could be of two forms, *viz*. zigzag-like and chair-like. For zigzag-like steps, the formation of edge states was predicted.[75] According to the data from scanning tunnelling microscopy studies, the energy of such states exceeds the Fermi energy by 0.02–0.15 eV.[77] STM images of zigzag-like steps show bright dots at the points of broken bonds.[78,79]

The activation energy of graphite oxidation at single-layer steps is somewhat higher than that at multilayer ones.[80] This fact can be explained by the bend of single-layer steps upon cleavage or under the pressure of the tip.[81] The stability of such structures has been analysed.[82]

The domain borders in STM images of HOPG are visible as wide helical structures.[76,83] The domain border for two crystallites with disorientation angle of 39° is shown in Fig. 11 *a*. A model proposed for this structure includes five- and seven-membered carbon rings. (Fig. 11 *b*).

The 2D defects observed in STM images of a HOPG surface include different superlattices. Hexagonal superlattices arising from the disorientation of the topmost graphite layers are described in the review[84] in great detail (Fig. 12), so we will just briefly concern this problem. Such superlattices are observed around dislocations[85,86] or can occur in the rotation of the

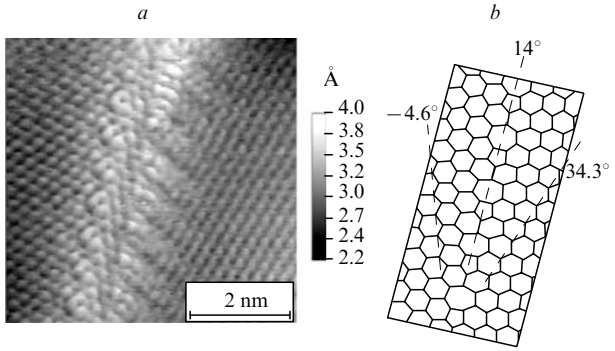



**Figure 11.** Image of the domain border obtained by STM (*a*), and its model (*b*).[83]

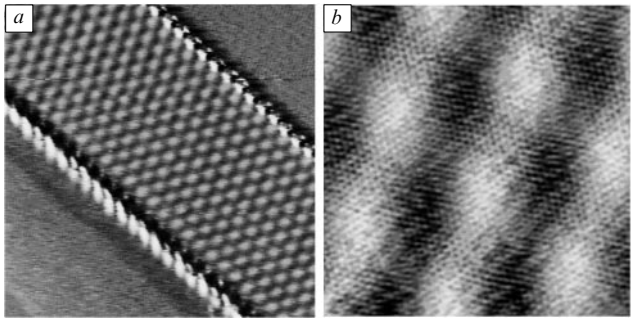



**Figure 12.** Images of superlattices on the HOPG surface (*a*) and superstructure area (*b*) obtained by STM.[85]
(*a*): $787 \times 787$ Å$^2$, $U = 480$ mV, $I = 0.6$ nA, the superstructure area is embraced by clear borders. The distance between the borders is 440 Å, the dimension of the area $> 1$ mm;
(*b*): $104 \times 104$ Å$^2$, $U = 210$ mV, $I = 0.6$ nA, superlattice period is $40 \pm 1$ Å and the angle of its rotation with respect to the graphite lattice is $28 \pm 1^\circ$.

topmost graphite layer.[85,87] Superlattices with periods from 1.7 up to 44 nm and height from 0.5 to 20 Å have been visualised. The reason for appearance of such defects is analogous to the Moire patterns in optics, which appear upon rotation of one periodic structure relative to another.[88,89] Due to the disturbance of layer packing, the asymmetry of maxima corresponding to the atoms in the A and B sites can differ within one superlattice unit cell.[90] Defects in the graphite lattice can lead to the vacancy formation in the superlattice.[91]

Lattices with different periods can be created on the surface of HOPG.[84] Such lattices can be applied in nanotechnology for the production of templates. For example, cobalt particles (1–5 nm) are adsorbed mainly on the nodes of the superlattice with the period of 3.8 nm.[92]

The appearance of periodic structures in STM images is not necessarily caused by the layer displacement. A superlattice with changing period was observed on the nanometer-size graphite sheet consisting of two layers.[93] The placement of a small graphite particle on the surface of the sheet resulted in the change in the lattice (Fig. 13). The appearance of this superstructure can be explained by the dimensional quantisation in a two-dimensional system. The change in the lattice parameter is due to the presence of a potential gradient in the system, which in turn is caused by the inclination of the sheet with respect to the bulk graphite. Dimensional quantisation was revealed in studies of etching pits with

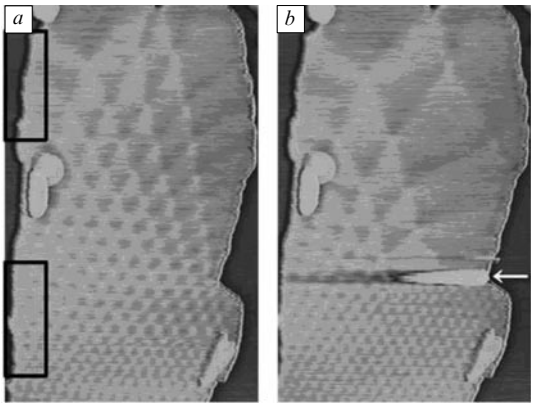



**Figure 13.** Images of superstructures on the nanometre-size graphite sheet obtained by STM before (*a*) and after (*b*) a graphite particle was placed on the sheet.[93]
(*a*): $U = 0.2$ B, $I = 0.7$ nA ($400 \times 250$ nm$^2$); layer height measured by STM image is $\sim 0.8$ nm in the top corner and $\sim 0.9$ nm for the bottom.

small diameter (< 10 nm) by scanning tunnelling microscopy.[94] The spectra of the pits located at a distance of 1 – 2 nm from each other have shown the splitting of the respective energy levels.

Finally, let us discuss superlattices arising due to the dislocation networks near the graphite surface. Most often, the dislocation networks observed in the STM images consist of triangular areas with sides of 100 – 300 nm.[95 – 98] Examination of triangle borders in the images with atomic resolution revealed a distortion of the hexagonal graphite lattice.[96] The surface corrugation increases on the borders.

On variation of the STM scanning parameters, images of the dislocation networks undergo certain changes. An increase in the tunnelling voltage leads to weakening of the contrast between the adjacent triangles.[96, 98] As the interlayer distances in hexagonal and rhombohedral graphite are similar and the Burgers vector of the network-forming dislocation lies in the [0001] plane, the contrast revealed in the STM images between the domains is not due to the surface topography. The presence of the step within the dislocation network area does not lead to its disruption or distortion. However the contrast between the perfect areas and the stacking fault areas changes (and can even be inverted) upon motion over the step.[98] For the explanation of this effect, a model has been proposed considering propagation of the electron wave along the graphite *c* axis together with the presence of defect areas below the surface. According to the proposed model, the STM scanning should reveal not only dislocations with the Burgers vector perpendicular to the base plane (screw dislocations [85, 86] and dislocation loops [99]), but also other types of dislocations.

Intensive mechanical pressure by the tip on the surface causes motion of the dislocations. Data are available indicating that the superlattices generated by the rotation of the topmost layer by less than 0.5° with respect to the substrate can transform to dislocation networks under the influence of the tip.[95] A triangular net presented in the STM image (Fig. 14 *a*) has transformed to the star-like structure (Fig. 14 *b*) after the change in the tunnelling voltage by 0.14 V.

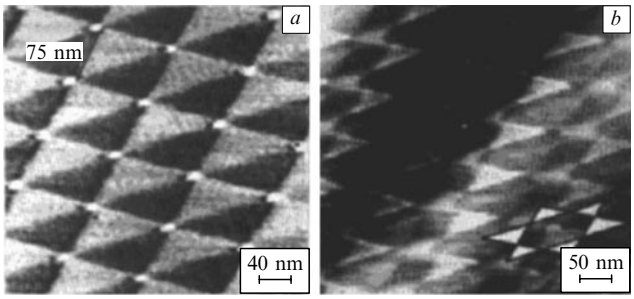



**Figure 14.** Dislocation network on the graphite surface (*a*) and a star-like structure (*b*).[96]
(*a*): $U = 0.24$ V, $I = 0.37$ nA, scanning frequency is 26 Hz;
(*b*): $U = 0.1$ V, $I = 2.4$ nA, scanning frequency is 26 Hz.

## V. Conclusion

Though the first STM image of atoms of the graphite surface was observed some 20 years ago, a consistent theory explaining why in some experiments only three atoms of the hexagonal cell are observed, and sometimes all six of them, has yet to be built. The existing theories on the nature of this effect still do not have the necessary experimental support.

Despite the obvious progress in the development of atomic force microscopy in the last 10 years, there are still only few AFM images of the defect areas of graphite. This is due to substantial difficulties of registration of extremely weak forces acting on the tip.

Methods of probe microscopy allow visualisation of the defects. However, the mechanisms of images formation sometimes remain obscure, for example, in the case of dislocations in the graphite. By the probe methods, the reactivities of different defect areas on the graphite surface were determined. With the use of STM and AFM microscopy, one can found preferable sorption sites for nanoparticles, as well as the state of adsorbates on the graphite surface.

This review was written with the financial support from the Russian Foundation for Basic Research (Project No. 04-03-32472-a).

## References

1. P L Walker (Ed.) *Chemistry and Physics of Carbon* (New York: Marcel Dekker, 1965)
2. A W Moore *Chem. Phys. Carbon* **69** 11 (1973)
3. A R Ubbelohde, F A Lewis *Graphite and Its Crystal Compounds* (Oxford: Clarendon Press, 1960)
4. G Binnig, H Rohrer, C Gerber, E Weibel *Phys. Rev. Lett.* **49** 57 (1982)
5. G Binnig, C F Quate, C Gerber *Phys. Rev. Lett.* **56** 930 (1986)
6. J Emsley *The Elements* (Oxford: Clarendon Press, 1991)
7. A S Fialkov *Uglegrafitovye Materialy* (Electrographite Materials) (Moscow: Energiya, 1979)
8. D D L Chung *J. Mater. Sci.* **37** 1475 (2002)
9. G Binnig, H Fuchs, C Gerber, H Rohrer, E Stoll, E Tossatti *Europhys. Lett.* **1** 31 (1986)
10. S Hembacher, F J Giessibl, J Mannhart, C F Quate *Phys. Rev. Lett.* **94** 056101 (2005)
11. T H Chang, C H Yang, M J Yang, J B Dottellis *Rev. Sci. Ins.* **72** 2989 (2001)
12. S Park, C F Quate *Appl. Phys. Lett.* **48** 112 (1986)
13. J Schneir, R Sonnenfeld, P K Hansma, J Tersoff *Phys. Rev. B* **34** 4979 (1986)
14. J I Paredes, A Martinez-Alonso, J M D Tascon *Carbon* **39** 476 (2001)
15. D Tomanek, S G Louie *Phys. Rev. B* **37** 8327 (1988)
16. R Sonnenfeld, P K Hansma *Science* **232** 211 (1986)
17. J R Hahn, H Kang, S Song, I C Jeon *Phys. Rev. B* **53** R1725 (1996)
18. R J Behm, H Rohrer, N Garcia (Eds) *Scanning Tunnelling Microscopy and Related Methods* (Dordrecht: Kluwer Academic, 1990)
19. H-J Güntherodt, R Wiesendanger (Eds) *Scanning Tunnelling Microscopy I (Springer Series in Surface Sciences)* (Berlin: Springer, 1992)
20. R Wiesendanger *Scanning Probe Microscopy and Spectroscopy. Methods and Applications* (Cambridge: Cambridge University Press, 1994)
21. S N Magonov, N-H Whangbo *Surface Analysis with STM and AFM* (Weinheim: VCH, 1996)
22. F Atamny, O Spillecke, R Schlögl *Phys. Chem. Chem. Phys.* **1** 4113 (1999)
23. S P Kelty, C M Lieber *Phys. Rev. B* **40** 5856 (1989)
24. H J Mamin, E Ganz, D W Abraham, R E Thomson, J Clarke *Phys. Rev. B* **34** 9015 (1986)
25. J Tersoff *Phys. Rev. Lett.* **57** 440 (1986)
26. S L Tang, J Bokor, R H Storz *Appl. Phys. Lett.* **52** 188 (1988)
27. E Tekman, S Ciraci *Phys. Rev. B* **40** 10286 (1989)
28. A Selloni, P Carnevali, E Tosatti, C D Chen *Phys. Rev. B* **31** 2602 (1985)
29. P Moriarty, G Hughes *Appl. Phys. Lett.* **60** 2338 (1992)
30. D Tomanek, S G Louie, H J Mamin, D W Abraham, R E Thomson, E Ganz, J Clarke *Phys. Rev. B* **35** 7790 (1987)
31. H P Lang, R Wiesendanger, V Thommen-Geiser, H-J Güntherodt *Phys. Rev. B* **45** 1829 (1992)
32. C H Olk, J Heremans, M S Dresselhaus, J S Speck, J T Nicholls *Phys. Rev. B* **42** 7524 (1990)
33. V Vignal, H Konno, M Inagaki, S Flandrois, J C Roux *J. Mater. Res.* **14** (1) 270 (1999)

34. P J Ouseph, T Poothackanal, G Mathew *Phys. Lett. A* **205** 65 (1995)
35. M-H Whangbo, W Liang, J Ren, S N Magonov, A Wawkuschewski *J. Phys. Chem.* **98** 7602 (1994)
36. A L Tchougreeff, R Hoffmann *J. Phys. Chem.* **96** 8993 (1993)
37. Yu N Moiseev, V I Panov, S V Savinov, I V Yaminsky *J. Vac. Sci. Technol. B* **12** 1690 (1994)
38. T A Land, T Michely, R J Behm, J C Hemminger, G Comsa *Surf. Sci.* **264** 261 (1992)
39. K S Novoselov, D Jiang, F Schedin, T Booth, V V Khotkevich, S Morozov, A K Geim *Proc. Natl. Acad. Sci. USA* **102** 10451 (2005)
40. T Sumomogi, K Hieda, T Endo, K Kuwahara *Appl. Phys. A* **66** S299 (1998)
41. C M Mate, G M McClelland, R Erlandsson, S Chiang *Phys. Rev. Lett.* **59** 1942 (1987)
42. T R Albrecht, C F Quate *J. Vac. Sci. Technol. A* **6** 271 (1988)
43. H Hölscher, U D Schwarz, O Zwörner, R Wiesendanger *Phys. Rev. B* **57** 2477 (1998)
44. F J Giessibl *Mater. Today* **8** (5) 32 (2005)
45. F J Giessibl *Rev. Mod. Phys.* **75** (3) 949 (2003)
46. N Sasaki, K Kobayashi, M Tsukada *Phys. Rev. B* **54** 2138 (1996)
47. S Fujisawa, Y Sugawara, S Ito, S Mishima, T Okada, S Morita *Nanotechnology* **4** 138 (1993)
48. F F Abraham, I P Batra *Surf. Sci.* **209** L125 (1989)
49. K Matsushita, H Matsukawa, N Sasaki *Solid State Commun.* **136** 51 (2005)
50. K Miura, N Sasaki, S Kamiya *Phys. Rev. B* **69** 075420 (2004)
51. C Horie, H Miyazaki *Phys. Rev. B* **42** 11757 (1990)
52. S Ciraci, A Baratoff, I P Batra *Phys. Rev. B* **41** 2763 (1990)
53. L Xu, X-W Yao, L-P Zhang, M-Q Li, F-J Yang *Phys. Rev. B* **51** 10013 (1995)
54. D Tomanek, G Overney, H Miyazaki, S D Mahanti, H J Güntherodt *Phys. Rev. Lett.* **63** 876 (1989)
55. N Sasaki, M Tsukada *Phys. Rev. B* **52** 8471 (1995)
56. L Xu, X Yao, L Zhang, M Li, F Yang *Phys. Rev. B* **49** 2875 (1994)
57. S Hembacher, F J Giessibl, J Mannhart, C F Quate *Proc. Natl. Acad. Sci. USA* **100** 12539 (2003)
58. A Schwarz, U D Schwarz, S Langkat, H Hölscher, W Allers, R Wiesendanger *Appl. Surf. Sci.* **188** 245 (2002)
59. C J Chen *Introduction to Scanning Tunnelling Microscopy* (New York: Oxford University Press, 1993)
60. H Hölscher, W Allers, U D Schwarz, A Schwarz, R Wiesendanger *Phys. Rev. B* **62** 6967 (2000)
61. A Tracz, A A Kalachev, G Wegner, J P Rabe *Langmuir* **11** 2840 (1995)
62. G Brauchle, S Richard-Schneider, D Illig, J Rockenberger, R D Beck, M M Kappes *Appl. Phys. Lett.* **67** 52 (1995)
63. E Bourelle, Y Tanabe, E Yasuda, S Kimura *Carbon* **39** 1557 (2001)
64. F Liu, Y Wang, J Xue, S Wang, S Yan, W Zhao *Phys. Lett. A* **283** 360 (2001)
65. D Marton, H Bu, K J Boyd, S S Todorov, A H Al-Bayati, J W Rabalais *Surf. Sci.* **326** L489 (1995)
66. Y Wang, Y Kang, W Zhao, S Yan *J. Appl. Phys.* **83** 1341 (1998)
67. R H Telling, C P Ewels, A A El-Barbary, M I Heggie *Nature Mater.* **2** 333 (2003)
68. J I Paredes, A Martinez-Alonso, J M D Tascon *J. Mater. Chem.* **10** 1585 (2000)
69. X Chu, L D Schmidt *Surf. Sci.* **268** 325 (1992)
70. K H Lee, H M Lee, H M Eun, W R Lee, S Kim, D Kim *Surf. Sci.* **321** 267 (1994)
71. N Takeuchi, J Valenzuela-Benavides, L Morales de la Garza *Surf. Sci.* **380** 190 (1997)
72. J Valenzuela-Benavides, L Morales de la Garza *Surf. Sci.* **330** 227 (1995)
73. H A Mizes, J S Foster *Science* **244** 559 (1989)
74. K F Kelly, E T Mickelson, R H Hauge, J L Margrave, N J Halas *Proc. Natl. Acad. Sci. USA* **97** 10318 (2000)
75. S Banerjee, M Sadar, N Gayathri, A K Tyagi, B Raj *Phys. Rev. B* **72** 075418 (2005)
76. W M Heckl, G Binnig *Ultramicroscopy* **42 – 44** 1073 (1992)
77. Z Klusek *Vacuum* **63** 139 (2001)
78. Y Kobayashi, K Fukui, T Enoki, K Kusakabe, Y Kaburagi *Phys. Rev. B* **71** 193406 (2005)
79. K Nakada, M Fujita, G Dresselhaus, M S Dresselhaus *Phys. Rev. B* **54** 17954 (1996)
80. X Chu, L D Schmidt *Carbon* **29** 1251 (1991)
81. F Atamny, T F Fissler, A Baiker, R Schllgl *Appl. Phys. A* **71** 441 (2000)
82. H V Roy, C Kallinger, K Sattler *Surf. Sci.* **407** 1 (1998)
83. P Simonis, C Goffaux, P A Thiry, L P Biro, Ph Lambin, V Meunier *Surf. Sci.* **511** 319 (2002)
84. W T Pong, C Durkan *J. Phys. D: Appl. Phys.* **38** R329 (2005)
85. T M Bernhardt, B Kaiser, K Rademann *Surf. Sci.* **408** 86 (1998)
86. B Feddes, I I Kravchenko, L E Seiberling *Scanning* **20** 376 (1998)
87. H Beyer, M Müller, Th Schimmel *Appl. Phys. A* **68** 163 (1999)
88. M Kuwabara, D R Clarke, D A Smith *Appl. Phys. Lett.* **56** 2396 (1990)
89. C Y Liu, H Chang, A J Bard *Langmuir* **7** 1138 (1991)
90. Z Y Rong, P Kuiper *Phys. Rev. B* **48** 17427 (1993)
91. Z Y Rong *Phys. Rev. B* **50** 1839 (1994)
92. J Xhie, K Sattler, M Ge, N Venkateswaran *Phys. Rev. B* **47** 15835 (1993)
93. Y Kobayashi, K Fukui, T Enoki, K Harigaya, Y Kaburagi, Y Hishiyama *J. Phys. Chem. Solids* **65** 199 (2004)
94. N S Maslova, A I Oreshkin, V I Panov, S V Savinov, A A Kalachev, J P Rabe *Solid State Commun.* **95** 507 (1995)
95. P J Ouseph *Phys. Rev. Lett.* **53** 9610 (1996)
96. S R Snyder, W W Gerberich, H S White *Phys. Rev. B* **47** 10823 (1993)
97. S R Snyder, T Foecke, H S White, W W Gerberich *J. Mater. Res.* **7** 341 (1992)
98. Y Kobayashi, K Takai, K Fukui, T Enoki, K Harigaya, Y Kaburagi, Y Hishiyama *Phys. Rev. B* **69** 035418 (2004)
99. P J Ouseph *Phys. Status Solidi A* **169** 25 (1998)